JJMIE

Volume 18, Number 3, September. 2024
ISSN 1995-6665
Pages 621- 633
https://doi.org/10.59038/jjmie/180315
Editor-in-Chief: Prof. Ali M. Jawarneh

Jordan Journal of Mechanical and Industrial Engineering

Transient Liquid Phase Bonding by Two-Step Heating Technique of IN939

Ruaa Hatem Kadhim[1*], Ahmed O AL-Roubaiy[1], H Omidvar [2]

[1] Department of Metallurgical Eng., College of Materials Engineering, University of Babylon, Babil, Iraq]
[2] Department of Materials and Metallurgical Engineering, Amirkabir University of Technology, Tehran, Iran

Received 11 Apr 2024 Accepted 22 Jul 2024

Abstract

Transient liquid phase **(**TLP) bonding was used to bond an IN939 superalloy utilizing a traditional, two-step heating process. The bonding process was carried out using BNi-2 foil with a 70-µm thickness as the interlayer in the first step at 1160 °C for 1 min and then at 1120 °C for different isothermal solidification times (50, 65, 80, and 95 min) in the second, also at 1120 °C for 80 min in conventional TLP bonding under vacuum furnace at a pressure of 10^{-5} torr. All the bonded specimens are then subjected to heat treatment and examined before and after heat treatment. A single-phase (isothermal solidification) was generated at the centerline after 80 minutes using a two-step technique. Due to insufficient bonding times, eutectic-products consisting of (gamma solid-solution), (Cr rich-boride), and (Ni rich-boride phases) formed in the centerline. The diffusion-affected zone also contained blocky- and needle-shaped boride precipitates in addition to the eutectic phases. The Vickers micro-hardness, and shear tests were done on the joints to evaluate their mechanical quality. The duration of isothermal solidification was shortened by using two-step TLP bonding. The hardness profile across the bond area was better than the conventional method and became more uniform after the heat treatment, and the shear strength was 631 MPa, and became 885 MPa after heat treatment, while about 479 MPa with the conventional TLP after heat treatment for the specimen with the isothermal solidification time of 80 min. After being subjected to a two-stage post-bond heat treatment, the microstructure becomes close to the base metals, as a result, a homogenizing microstructure forms across the joint. With increased bonding times, all of the bonds' shear strengths increased, and the hardness distribution across the bond area was better than the conventional technique and following the heat treatment, became more uniform. The bond shear strength was enhanced after the heat treatment because a significant γ-'phase developed in the bond area.

Keywords: Two-step heating TLP bonding, Inconel 939, Heat treatment, Microstructure, Shear strength, Micro-hardness.

1. Introduction

The hot section parts of the gas turbine, including the stationary and rotary components, are subjected to thermal and mechanical fatigue, oxidation, creep, hot corrosion, and damage to foreign objects during gas turbine operations. So, to achieve stable operation in an aggressive environment, various types of superalloys must be used [1, 2, 3]. Joining is necessary when manufacturing these alloys, and a significant amount of work has been done on many different types of techniques that can be used to successfully fabricate them [4]. Nickel-based superalloys' weldability is mostly determined by the amount of Al and Ti. Precipitation hardening of nickel-based super alloys is extremely difficult to weld due to their great sensitivity to solidification cracking within the fusion zone and heat-affected zone (HAZ) during welding or post-bond heat treatment [5-8]. Also, diffusion bonding and brazing methods are limited in their use for the repair or fabrication of nickel-based super alloy parts due to problems connected with them. During the brazing process, brittle phases may form in the joint area, weakening the joint's properties [9, 10]. To resolve these issues, Duvall et al. achieved transient liquid phase (TLP) bonding [11]. Materials that are difficult to join using traditional techniques are best joined using TLP bonding. There are three steps in conventional TLP models: dissolution, isothermal solidification, and solid-state homogenization. The base metal generally dissolves over several minutes due to the melting-point depressant (MPD) components' short-range diffusion. Long-term diffusion occurs during the isothermal solidification stage, which takes longer, ranging from minutes to hours depending on the bonding temperature, and type of interlayer. The homogenization step, on the other hand, is performed to enhance the joint's qualities. [12-15]. The formation of the joint in the TLP bonding process is dependent on the isothermal solidification of the liquid phase at a constant bonding temperature. According to the studies of Mac Donald and Eager [16], isothermal solidification may take a long time to complete. TLP's uses in many industries are limited as a result of this. Shirzadi, and Wallach [17]

* Corresponding author e-mail: ruaa.hatem@uobabylon.edu.iq.

devised a unique approach for TLP bonding that uses a temperature gradient (TG) across the bond- line rather than keeping a constant temperature during bonding. One of the most significant advantages of this novel technique is that bonding time is predicted to be significantly reduced compared to conventional TLP bonding. Additionally, TG over the liquid phase can lead to the production of a non-planar interface, which increases bond strengths due to the increased metal-to-metal contact, in contrast to the planar interfaces associated with conventional- -TLP bonding. The interfaces may limit the bond strength, even though TG-TLP bonding can result in a strong joint. As a result, Wang- et al. [18] developed a technique for TLP bonding that uses two-step heating to produce a homogeneous joint. The first stage of this procedure is done at a high temperature for a short period. The joint is then maintained at a lower temperature until the second process of isothermal solidification is finished. At a high temperature, the liquid phase forms, and at a low temperature, it begins to solidify. The equilibrium is broken when the temperature drops and a constitutional-super-cooling forms at the solid/liquid boundary. In contrast to the unidirectional interface migration observed during TG- TLP bonding, the two non-planar interfaces move in opposite directions and meet in the liquid phase's core. A homogenous joint is created by combining the high-angle grain boundaries. Only a few research investigations in the field of two-step-heating TLP bonding have been done to date. To present, the majority of research has focused on the conventional TLP bonding procedure. A similar joining of IN939 using two-step heating in TLP bonding has not been described in earlier studies. Furthermore, there was no comparison of mechanical characteristics with conventional TLP bonds. There was also no research on the influence of heat treatment of base metals (IN 939) on TLP bonding using two-step heating. Additionally, the microstructure and mechanical characteristics of TLP bonds are compared before and after heat treatment using the two-step heating technique.

2. Experimental

2.1. materials

The as-cast polycrystalline Ni-base superalloy (IN939), in the form of (50×100×100) mm plates, was used as the base metal. In addition, BNi-2 was used as a filler metal in the form of a 70μm thick-foil. Table 1 shows the chemical compositions of the materials utilized in this investigation, which were evaluated using Optical Emission Spectroscopy (OES). The filler alloy's liquid and solidus-temperatures were 999°C and 971°C, respectively [19].

2.2. Bonding procedure

The as-received plates were sectioned into specimens with dimensions of (10 × 10 × 5) mm using NC wire electro-discharge machining. To ensure the removal of an oxide layer created through the machining procedure, all specimens were prepared with SiC paper to an 800-grit finish for bonding. The specimens and filler were cleaned in an ultrasonic acetone bath for about 15 minutes after grinding. The filler alloy was sandwiched between the cleaned specimens' mating surfaces. To prevent the entire assembled pieces from moving during TLP bonding, a fixture fabricated from St37 was utilized, as illustrated in Figure 1b. Only the specimen weight, which was the same for all samples, applied pressure to the assembled parts. The assembly was then put in a vacuum furnace at a pressure of around 10^{-5} torr. Table 2 lists the bonding variables for all the samples produced using the traditional TLP bonding technique and the two-step heating method. The parameters were selected based on previous studies, and several experiments were done step by step to reach the current parameters. After bonding, all the bonded specimens are then subjected to the heat treatment of IN939 (solution treatment at 1160 °C for 4 h, then rapid air cooling, and aging at 845 °C for 16 h, then air cooling) [20, 21]. Figures (1 a) depict a schematic illustration of heat treatment. The EDM was used to section the bonded specimens perpendicular to the bonding zone for microstructure investigation. Then the mounting operation was carried out. After mounting, grinding with SiC paper grades was used to grind the surface of the specimen. Thereafter, they were polished using paste. Finally, the diamond paste was used for final polishing. Following the polishing operation, the specimen was immersed for 5 seconds in a marble etching solution (10 g $CuSO_4$, 50 ml HCL, 50 ml H_2O) to study the microstructure in the bonding area. The electrochemical reagents (45% butanol, 10% perchloric acid, and 45% acetic acid) were used for etching the specimens under the conditions (5-10 vs. 20s) to study the size, and distribution of γ′ precipitates [8]. After that, samples were examined before and after heat treatment.

Table 1. The Chemical Compositions of the Base Metal and the Filler-Alloy (Wt%)

Elements (Wt%)																		Alloy
Si	Mn	Cr	Mo	Cu	Fe	Co	Ti	Al	Nb	W	C	Ta	Zr	B	V	Cu	Ni	
0.04	0.04	22.4	0.05	0.01	0.12	19.2	3.70	1.84	1.11	2.04	0.14	1.3	0.08	-	0.01	0.01	Base	IN939
4.32	0.015	5.92	-	-	2.90	0.054	-	-	-	-	0.034	-	-	1.89	-	-	Base	BNi-2

Table 2. Parameter used in TLP-bonding

Sample	Short-time heating stage		Isothermal solidification stage	
	Temp.(c°)	time(min)	Temp.(c°)	time(min)
D-50	1160	1	1120	50
D-65	1160	1	1120	65
D-80	1160	1	1120	80
D-95	1160	1	1120	95
DC-80			1120	80

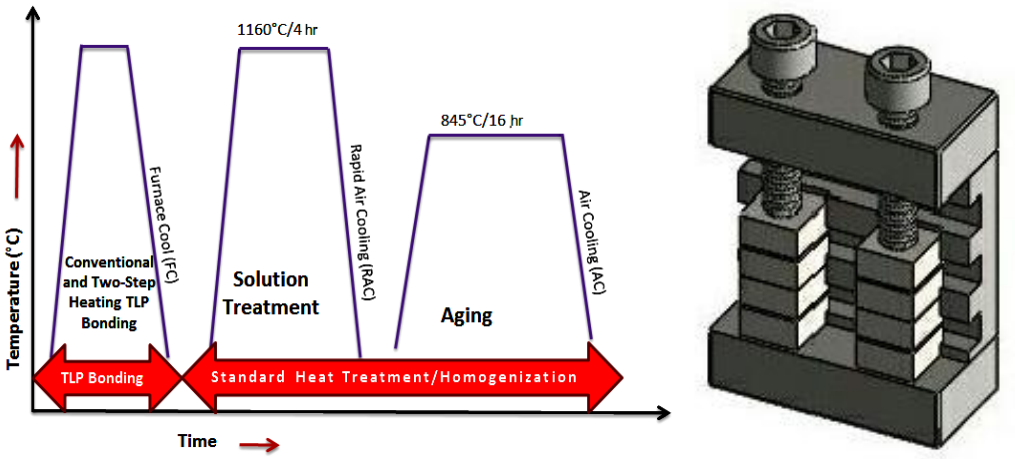

a) b)

Figure 1. a) Schematic illustration of Standard heat treatment, b) design of the joint and fixture

2.3. Mechanical testing

Shear tests and microhardness were used to analyze the mechanical characteristics of the TLP bonding before and after heat treatment. A Vickers micro-hardness tester was used to evaluate how the hardness changed over the joint region about the distance from the bond contact. Microhardness measurements were made over the joint region by the ASTM E384 standard using a 50 g force applied for 10 seconds [22]. Before the hardness test, appropriate grinding and polishing operations were done. To determine the mean values of three areas, the hardness value at each position was averaged across at least five measurements. Using a tensile machine with a speed of 1 mm/min, a shear test at ambient temperature was carried out by ASTM: D1002 [23]. During the tensile testing, the shear force was applied to the joints using a fixture. To avoid stress concentration, sample surfaces were ground before this test. The mean values of three tests were performed on 10×10×10-mm samples at each condition, and the results are reported. OM and SEM were used to investigate the fracture surfaces. A schematic of the manufactured fixture for the shear test is shown in Figure 2.

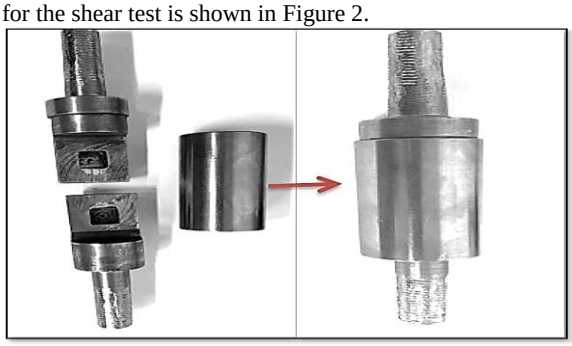

Figure 2. The fixture schematic diagram and the manufactured fixture for shear test.

3. Results and Discussion

3.1. Microstructure of TLP bonded joints

The base metal was Ni-based superalloy IN939, which was bonded. Figure 3 shows the microstructure of the bonded specimen after 50 minutes of time in the second step. In the TLP bonding-area of specimen (D-50), it can be seen that the microstructure consists of four different zones.

3.1.1. Athermal Solidification Zone (ASZ)

This zone is formed as a result of the solidification of the residual liquid in the bond line during the cooling of the specimen to room temperature. The driving force for this zone is cooling. Due to inadequate melting-point depressant (MPD) diffusion from the liquid filler into the surfaces, the liquid filler in the bond line does not have enough time to solidify fully isothermally, and as a result, it is composed of the eutectic products of non-isothermal solidification. From the FE-SEM secondary and backscattered electron images shown in Figure 4 (a) and (b), it can be seen the TLP-bonded area with higher magnification for the centerline eutectic (ASZ) in (c) and (d), and the different phases that are found in the eutectic of the specimen (D-50). The FESEM/EDS analysis was utilized to determine the composition of available phases at higher magnification to know more about the phases within the eutectic products. As shown in Table 3 for the zones (A to D). In Figure 4 (d), the point "D" is primary carbides (6.50Ni, 1.90Cr, 2.28Si, 1.19Mo, 0.48Al, 37.18Ti, 0.13Fe, 0.70Co, 20.51B, 5.81Nb, 2.25W, and 21.06C). Table 3 shows the results of the EDS compositional analysis, which indicate that the eutectic products are divided into three phases: the γ- solid solution, Cr and Ni phases- rich boride. The formation of the same solidification phases has been reported in TLP-bonded IN939 and other Ni-base superalloys in the references [24–26]. The residual liquid interlayer's high boron content and the substantial quantities of nickel and chromium it contains make it necessary for the eutectic products to form, leading to the formation of the eutectic products, which included nickel- and chromium-rich $M_{23}B_6$-borides, nickel-based solid-solution phases, and M_5B_3-borides.

During isothermal solidification, the γ ----phase solid solution is the first to form from the melting surfaces into the melt in the bond area at the bonding temperature, but when there isn't enough time to finish solidification isothermally, the athermal solidification begins. The microstructure development in the ASZ can be significantly controlled by solidification; examples include the creation

of the dendritic structure and solute partition. Solidification occurs in the direction of the base metals toward the bond line. When studying the solidification sequence of the remaining liquid after cooling, the microstructure of ASZ may be described. When a γ -solid solution in the form of dendrites grows from the liquid/solid interface during cooling, the solute elements with a partition coefficient less than one (K<1) are rejected into the liquid (melt). As a result, these solute components become more concentrated. and exceeds the solute's solubility limit in the γ-solid solution phase. As a result, between dendrites, secondary solidification constituents form. Since then, according to the binary Ni-B equilibrium phase diagram [27], the solubility of boron in nickel has been about 0.3 percent. Because of this, B dissolves far less easily in Ni and Cr than Si does.

B is thus rejected into the remaining liquid, changing its eutectic composition. Consequently, solidification continues, resulting in the formation of a binary eutectic made up of the γ -phase, nickel boride, and chromium boride. Si becomes more concentrated in the residual liquid due to the insolubility of Si in boride phases, this is in agreement with the reference [28]. As a result, the liquid becomes even more Si-enriched, yielding a product (eutectic) composed of γ-phase, Ni and Cr-rich borides, and Ni-rich silicide, in agreement with the reference [29]. The reaction of eutectic during the cooling of IN939 TLP bonded with BNi-2 filler alloy is as follows, based on the above results:

$$L \rightarrow \gamma + L \rightarrow \gamma + NiB + CrB$$

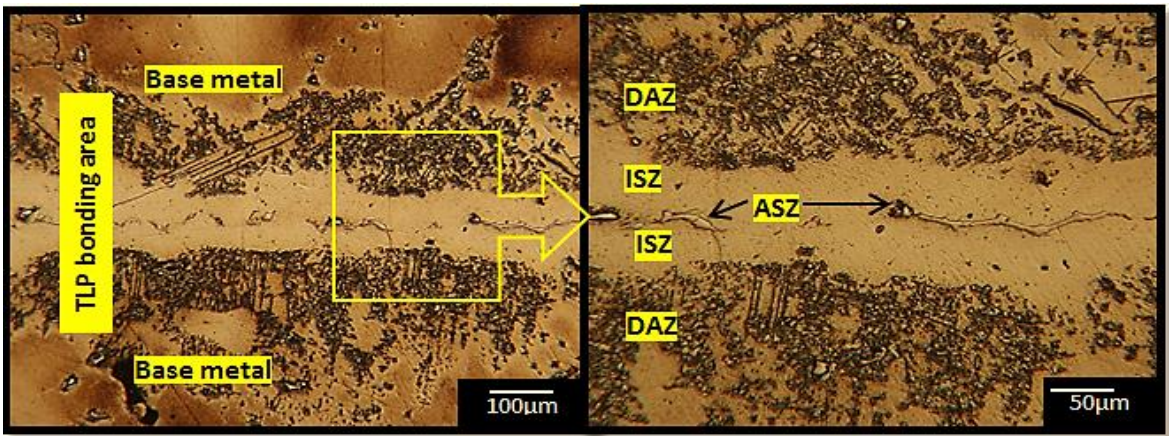

Figure 3. Optical micrographs of the TLP bonded area of specimen D-50

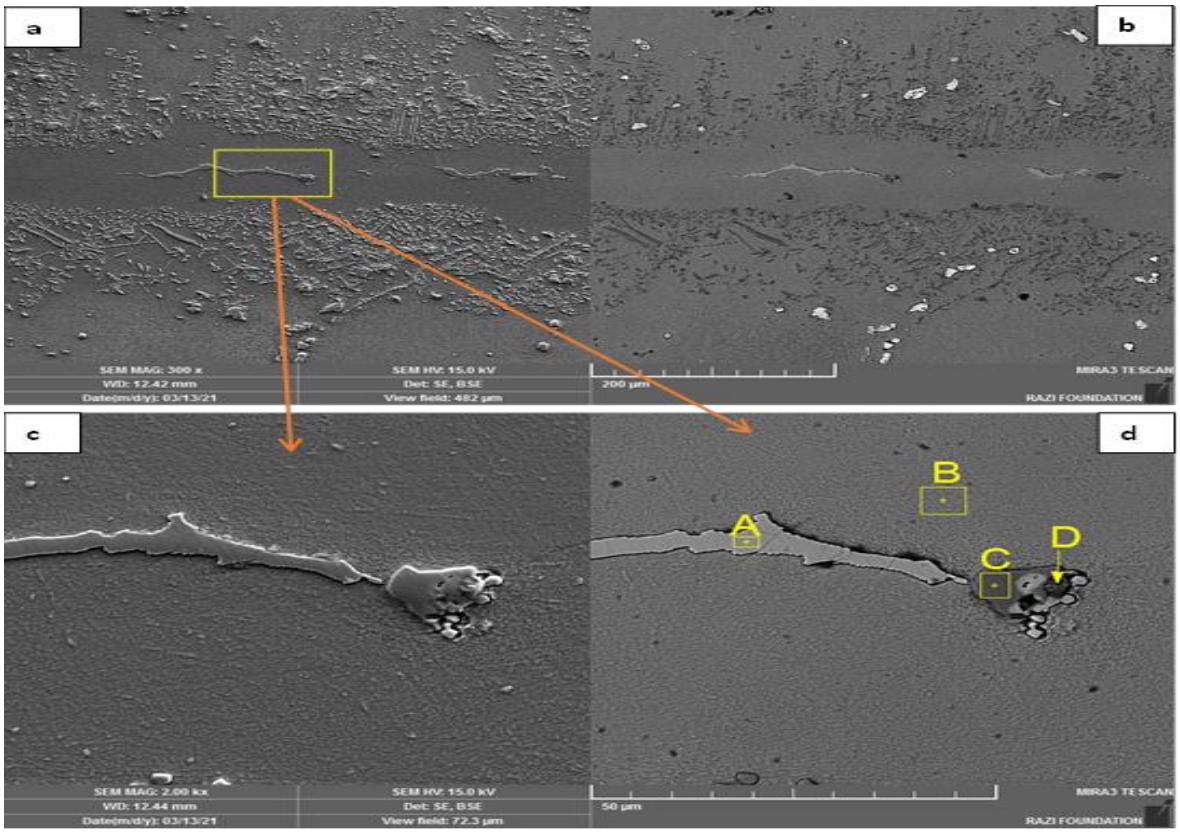

Figure 4. FE-SEM of the Specimen (D-50) (a) and (b) Secondary and Backscatter Electron Images Showing Different Zones in the Solidified Area. (c) and (d) Secondary and Backscattered Electron Images at Higher Magnification Showing Available Phases (A-D) in Eutectic Products in the Centerline of the Joint

3.1.2. Isothermal Solidification Zone (ISZ)

This zone's microstructure consists of a solid-solution phase rich in nickel that contains elements including Mo, Ti, Al, and Nb that aren't present in the TLP filler alloy composition. Because there is no solute rejection at the liquid-solid contact, The creation of a second phase does not occur in this zone [7, 30]. The ISZ is a single-phase γ -solid solution, according to the results of SEM/EDS analysis (B in Figure (4 d)) in Table 3. Figure 5 shows the microstructure of the TLP bonded for 80 minutes in the second stage using FE-SEM secondary and backscattered electron images for specimen D-80. The phase solid-solution is the only phase generated at the joint centerline, as seen in this figure. As a result, the bond region only has ISZ in the centerline and no eutectic products.

3.1.3. Diffusion affected zone (DAZ)

Figure 6 illustrates the FE-SEM secondary and backscattered electron images for the specimen (D-50) with higher magnification for the microstructure of DAZ. As shown in Figure 6, "E" is blocky and "H" is needle-shaped precipitates; "G" is the solid solution matrix in DAZ; and "F" is white particles; these were base metal primary carbides (0.87Ni, 0.24Cr, 0.47Si, 16.66Ti, 0.12Co, 16.32B, 1.93W, and 15.99Nb); this is in agreement with the literature [31, 32]. the existence of certain borides produced in the near base metal and the diffusion of boron from the filler metal, like Cr in IN939, lead to the precipitation of these borides during the dissolution and isothermal solidification stages. These second phases first have a blocky shape in the region near the isothermal solidification zone and then change to a needle shape by moving away toward the base metal zone. This is in agreement with the literature [24, 33]. The chemical composition of the second phase and the matrix in the diffusion-affected zone are shown in Table 4.

Table 3. chemical composition (at%) for all the labeled zones that shown in figure 4.

	Ni	Cr	Si	Mo	Al	Ti	Fe	Co	B	Nb	W	Predicated phase
A	48.95	1.11	5.70	1.94	0.26	3.86	0.22	3.16	22.45	10.40	1.97	Ni-rich borides
B	61.84	9.43	0.79	0.0	0.50	1.78	0.82	5.99	13.48	2.90	2.47	γ- solid solution
C	2.29	46.03	0.07	2.55	0.24	1.41	0.22	2.05	37.26	2.75	5.14	Cr-rich borides

Table 4. chemical composition (at%) for the points that shown in Figure 6

	Ni	Cr	Si	Mo	Al	Ti	Fe	Co	B	Nb	W	Predicated phase
E	1.44	61.96	0.06	1.28	0.36	0.32	0.09	2.11	28.05	0	4.34	Blocky Cr- rich borides
H	6.63	70.39	0.09	0.42	0.64	0.79	0.13	3.17	10.03	2.89	4.50	Needle Cr-rich borides
G	46.16	13.69	0.13	5.62	1.62	2.58	0.33	13.37	10.85	0	5.64	Gama matrix

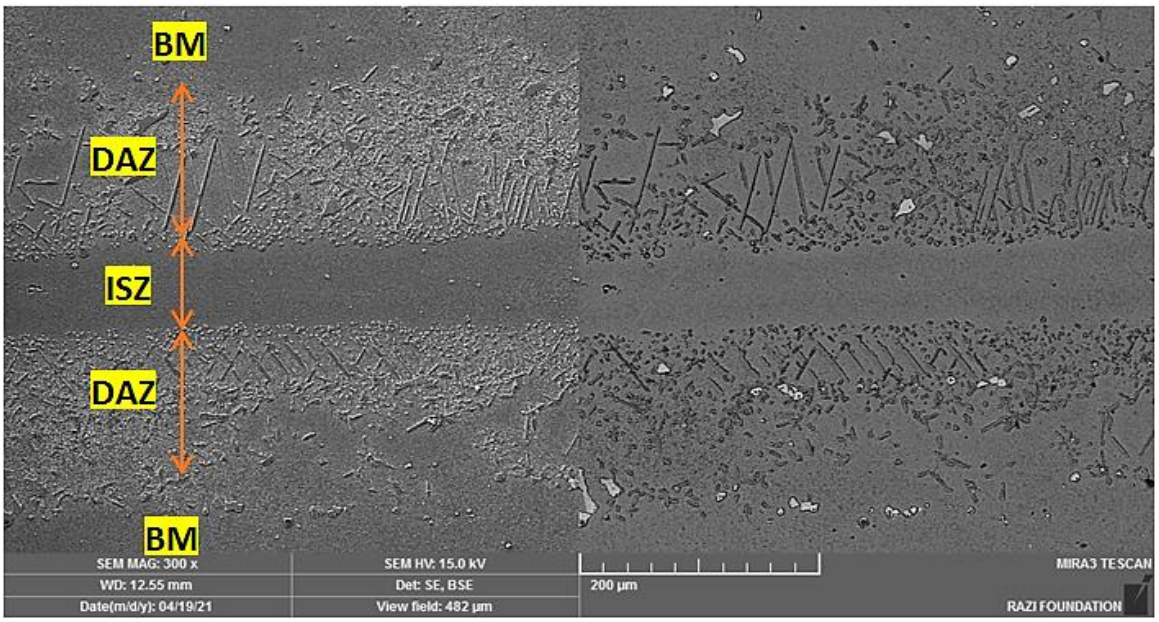

Figure 5. FE-SEM images of the specimen (D-80)

3.1.4 Gama prime precipitates at the bond line

In the IN939 superalloy, the distribution of Gama prime precipitates (γ′) in the base metal and bond line is shown in Figure 7 for the specimen (D-80). Figure 8 shows the γ′ precipitates along the bond area from the centerline (ISZ) to the base metal of the specimen (D-80); this condition achieved full isothermal solidification. Figure 7 shows that the γ′ in the centerline is less than that in the base metal. As previously stated, the presence of γ′ in the bond line indicates dissolution of the base metal elements (Al, Ti, and Mo) and enrichment of the molten phase with these elements in the isothermal solidification zone. Based on these findings, the TLP-bonded joint of IN939 with BNi-2 as a filler alloy at an 80-minute holding time in the second step has a centerline structure (ISZ) that is similar to the base metal structure.

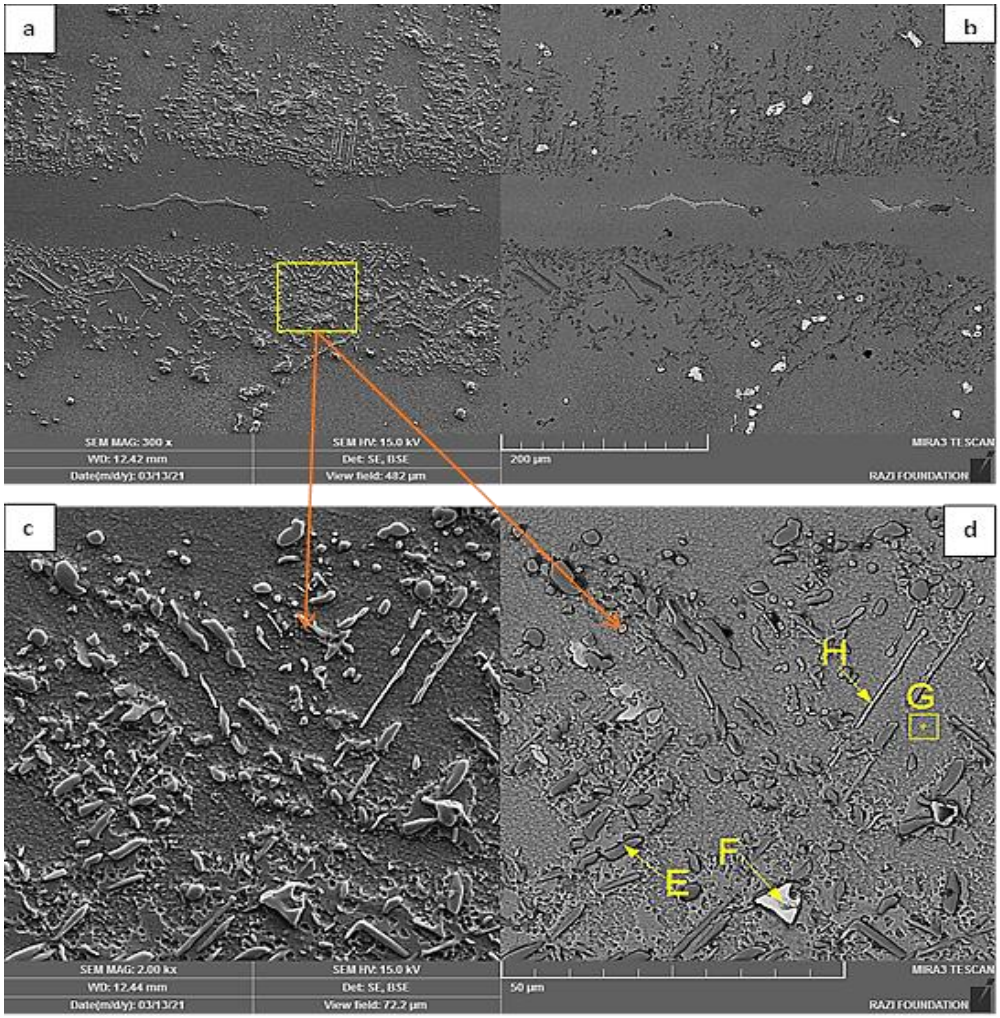

Figure 6. FE-SEM Secondary and Backscattered Electron Images for the Specimen D-50 in (a) and (b), with Higher Magnification for the Microstructure of DAZ in (c) and (d)

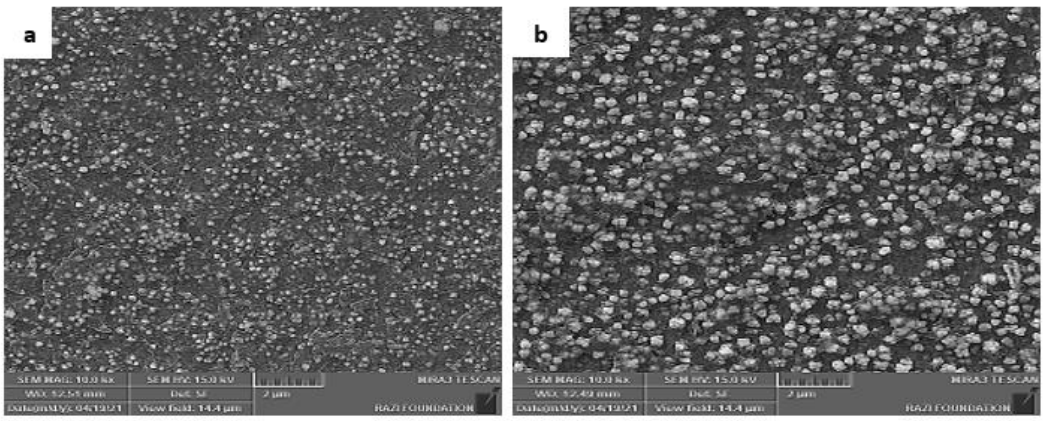

Figure 7. FE-SEM images for the γ′ precipitates in the specimen S-80 in (a) ISZ (centerline) (b) base metal zone.

3.2. Effect of Two- step Technique and Bonding Time on the Microstructures of TLP Bonds

On the IN939 specimens, bonding was carried out. The period required to complete isothermal solidification and prevent the formation of centerline eutectic phases at a specific bonding temperature and gap size determines how well TLP bonds. Figure 9 illustrates the microstructure examination of bonded joints. According to this figure, the joint had eutectic products in the second phase after 50 minutes. So, through the cooling process from bonding temperature to room temperature, the microstructure of the joints is divided into four main zones: the ISZ, ASZ, DAZ, and BM zones. Due to increasing B and Si diffusion into the substrate, the average width of the DAZ region widened with increased holding time. In addition, the precipitates in the DAZ were larger, and the ISZ's width widened, as shown in the figure. In this investigation, full isothermal solidification of the joints was obtained in 80 minutes in the second step (two-step TLP bonding). Despite this, isothermal solidification did not occur completely, and a centerline eutectic was discovered for the standard TLP specimen after 80 minutes of one-step bonding, as shown in Figure 9: (c and e). This indicated that using two-step heating for TLP bonding might minimize the time necessary for isothermal solidification. This study's findings are in agreement with earlier research [34, 35].

A two-step heating TLP method was used to generate an imposed supercooling at the interface as a result of the temperature reduction. This caused the interface to become unstable, producing a form that is complex and non-planar [36]. Although it has been demonstrated that an unstable interface benefits from strong bonding, severe instability should be avoided to prevent an unsuitable microstructure. The interface has grown in both cellular and wavy shapes as a result of the low temperature. It has been reported that increasing interfacial curvature can reduce solidification time [37] and that enhanced interfacial curvature can speed up the movement of the liquid/solid interface in the two-step heating process [38]. As a result, isothermal solidification happens more quickly in the two-step heating process while the interface was planar for the bonding produced by conventional TLP bonding.

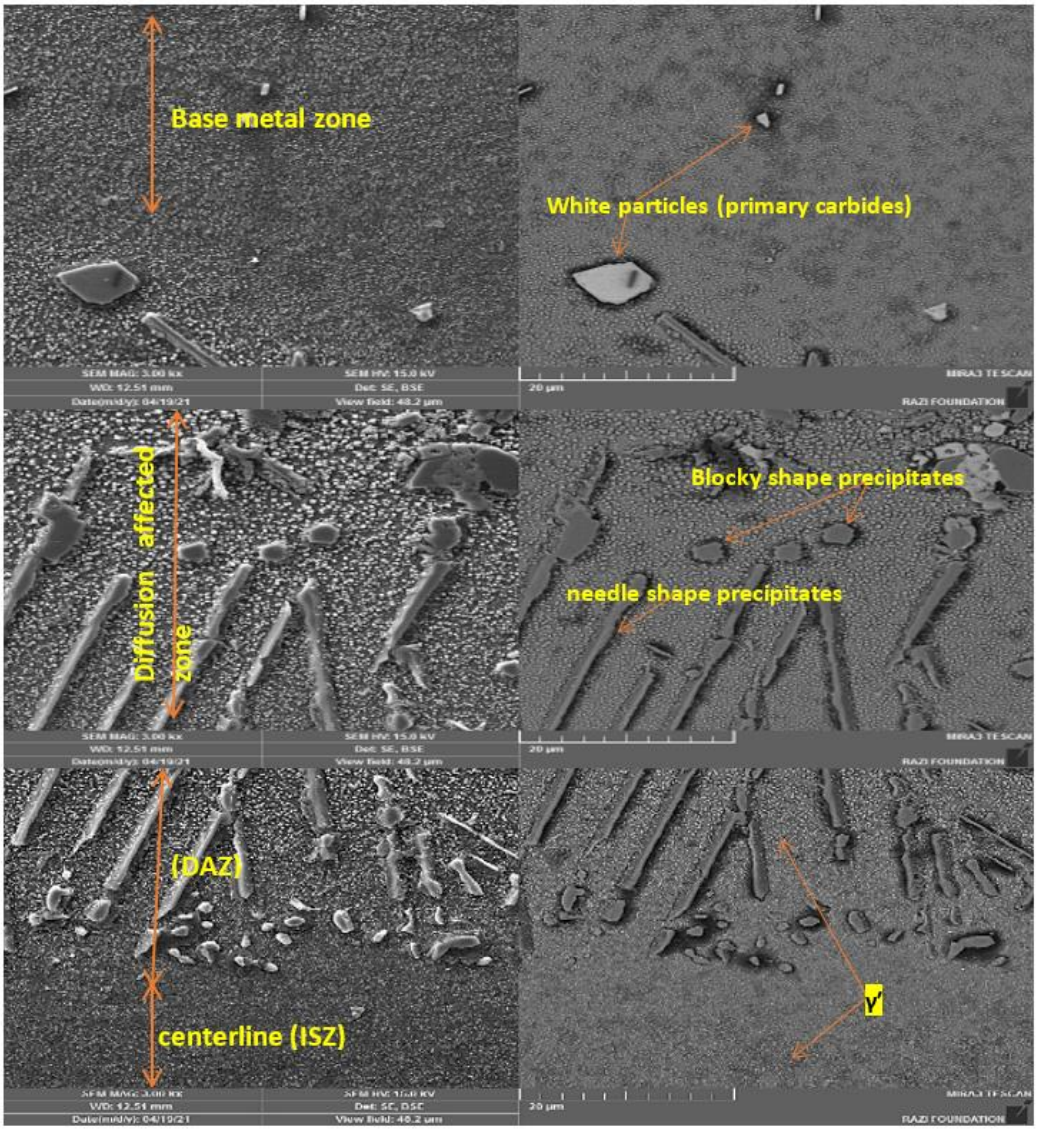

Figure 8. FE-SEM Secondary and Backscattered Electron Images for the γ′ Precipitates of Specimen D-80 from Centerline Side to Base Metal Side

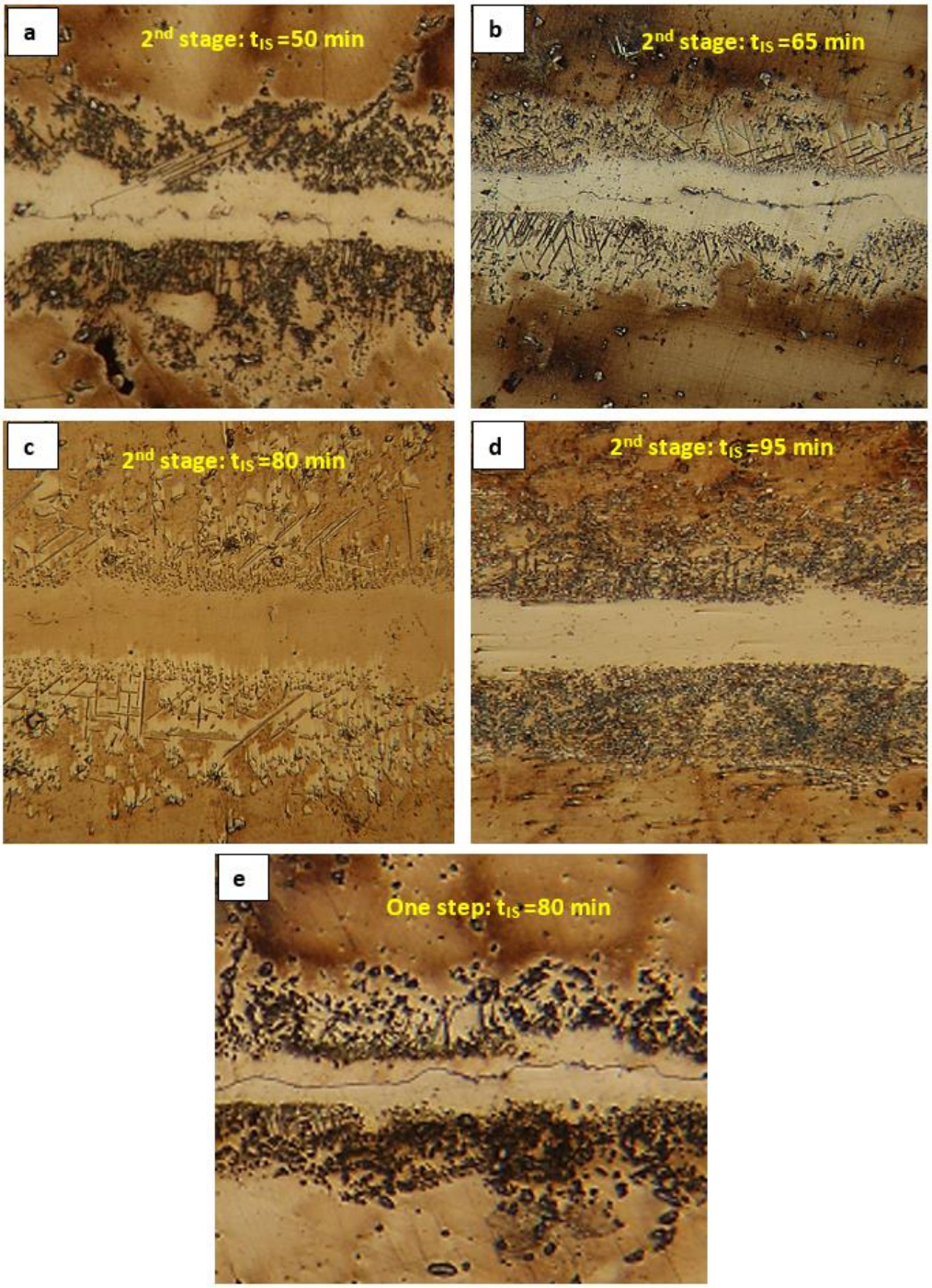

Figure 9. OM of two-step heating TLP bonding of similar IN939 : a) specimen D-50, b) specimen D-65, c) specimen D-80, d) specimen D-95, and e) specimen DC-80

3.3. Characterization of post-bond heat treated TLP bonds

The bonds of IN939 are subjected to two stages of post-bond heat treatment: solution treatment at 1160 °C for 4 hr, then rapid air cooling (first stage); and aging treatment at 845 °C for 16 hr, then air cooling (second stage). After being subjected to the two-stage PBHT, the bond line of all the heat-treated specimens also contained the only phase (γ solid solution), so was free from any second phase in this region. This is due to the complete interdiffusion between the base metal and interlayer during the solution treatment (first stage). According to this, the volume fraction of γ′ increases, and the PBHT causes coarsening of precipitating in the base metal zone during the second stage of aging treatment. FE-SEM image for the heat-treated joint of the specimen D-80 is shown in Figure 10. Figure 11 shows FE-SEM images at higher magnification for the bond line region and base metal region for the specimen (D-80) after heat treatment. From the results of this figure, the joint region had a considerable increase in the formation of γ′ - precipitates, which may have been caused by increased Al, Ti, Co, and Ta diffusion from the base metals. The precipitates in the base metal zone were coarse and spherical under heat treatment conditions; this is in agreement with the references [30,39,40].

3.4. Mechanical properties of TLP bonded and post-bond heat treated joints

3.4.1. Micro-hardness measurement

The hardness profile of the similar IN939 TLP bonds obtained by the two-step heating technique for specimen D-50 is shown in Figure (12 a). This specimen contains four zones: the ASZ, ISZ, DAZ, and BM zones. The average micro-hardness values in different zones are shown in this figure. The high hardness of ASZ is due to a high-hardness Ni- and Cr-rich boride that is present near the centerline of the joints. In specimen D-80, the ASZ was completely removed. So, the centerline contained only ISZ, as shown in Figure (12 b). the increasing concentration of solid solution-strengthening elements in the base metals (Al, Ti, and Co), the average hardness of ISZ was lower than that of the base metals. lower concentrations of these alloying elements in the ISZ (bond line) because of insufficient diffusion of alloying elements. As shown in the figure, all of the samples have high DAZ hardness values. This is because the zone contains hard, brittle boride precipitates, this is in agreement with the references [31,33]. whereas at 80 minutes in conventional TLP, the centerline contains ASZ due to insufficient time to complete isothermal solidification. The hardness of all the different zones in the specimen DC-80 is shown in Figure (12 c). All specimens were heat treated using solution treatment and aging treatment on IN939 to homogenize the hardness along the bond area to remove ASZ and reduce the hardness values of DAZ in the TLP bonds, this is in agreement with the references [30,32]. The results of the micro-hardness values after heat treatment are shown in Figure (12 d).

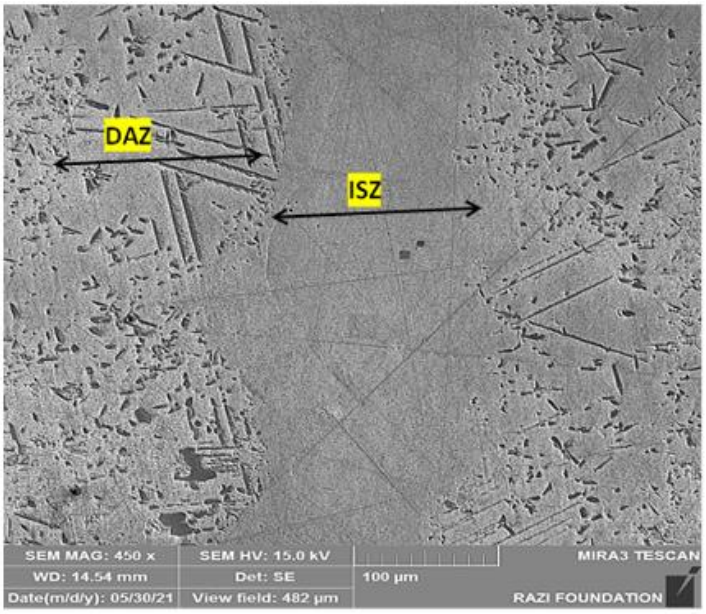

Figure 10. FE-SEM Image of the Bond Area for the Specimen D-80 After Standard Heat Treatment

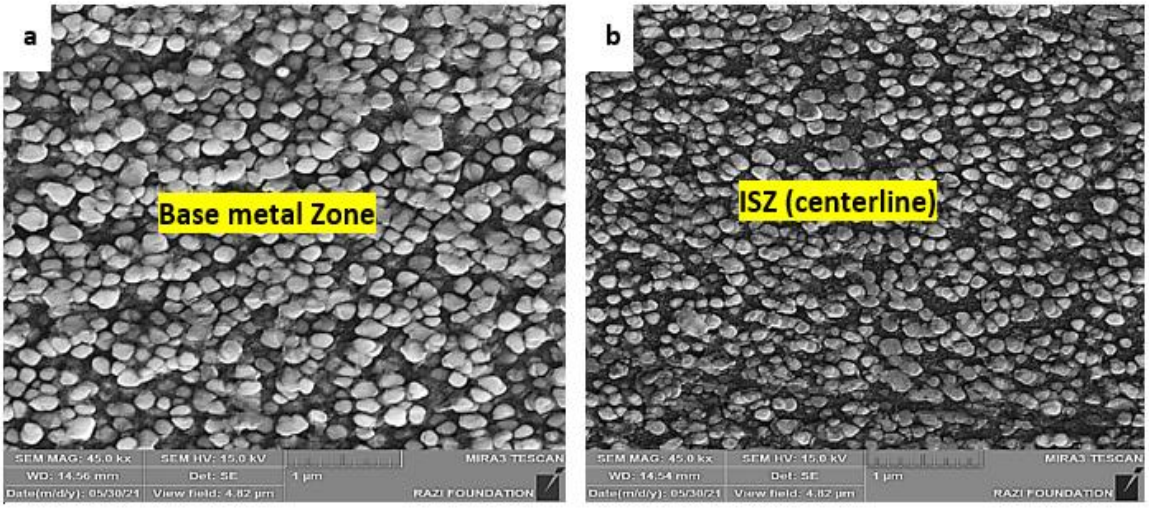

Figure 11. FE-SEM Images at Higher Magnification for the γ′ Precipitates in the Specimen (D-80) in (a) Base Metal Zone, (b) ISZ (Centerline)

3.4.2. Shear test

The shear strength of heat-treated specimens of IN939 TLP bonded using a two-step heating technique with different isothermal solidification times (50, 65, 80, and 95 min) is illustrated in Figure (13 a). According to the figure, shear strength increased as bonding time increased from 50 to 95 minutes, and for heat-treated specimens, shear strength increased as isothermal solidification time increased. This is because the amount in the centerline has increased. Compared with the non-heat-treated specimen D-80, the shear strength of the specimen without heat treatment is lower than that of the heat-treated TLP-bonded. This is due to the formation low amount of γ′ in the centerline. Also, to compare TLP-bonding of similar IN939 using the two-step heating technique with conventional TLP after heat treatment, the shear strength of TLP using the two-step heating technique is higher than the conventional TLP at the same time, as shown in Figure (13 b). The results of the shear test are in agreement with the references [30,33]. Interlocking two non-planar interfaces increased the contact area (metal to metal) and aided in the formation of a joint with improved mechanical characteristics.

The shear fracture surface FE-SEM images for specimen D-80 after bonding and post-bond heat treatment are shown in Figures (14) and (15), respectively. The study found that the fracture propagated through the areas of specimen D-80 (full isothermal solidification in these conditions) (ISZ and DAZ). As previously stated, the number of precipitates in the bond region is the most important determinant of shear strength. Because the secondary phases in the DAZ are not evenly distributed over the interface between the ISZ and the BM zone, they have less of an influence on joint shear strength. So, the crack propagated through the soft bond area. The fracture surface of heat-treated specimen D-80 is shown in Figure (15). The fracture surface's FE-SEM images show that the interface and base metal both showed random fracture growth, which was compatible with the heat-treated joint's high-strength.

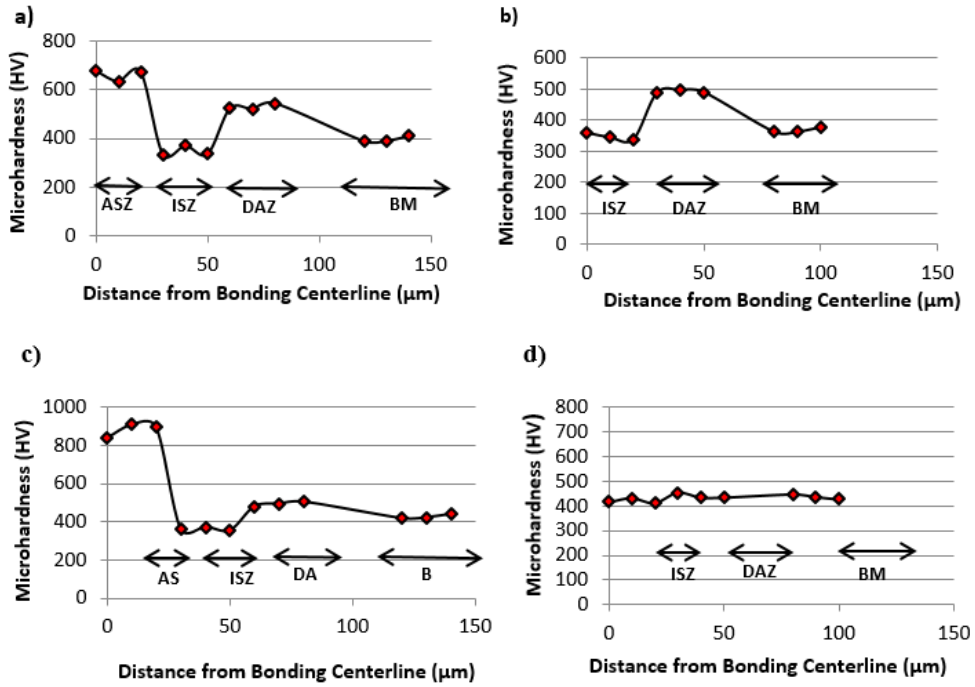

Figure 12. a) Hardness profile of the specimen D-50, b) Hardness profile of the specimen D-80, c) Hardness profile of the specimen DC-80 conventional TLP bond, and d) Hardness profile of the heat-treated specimen D-80

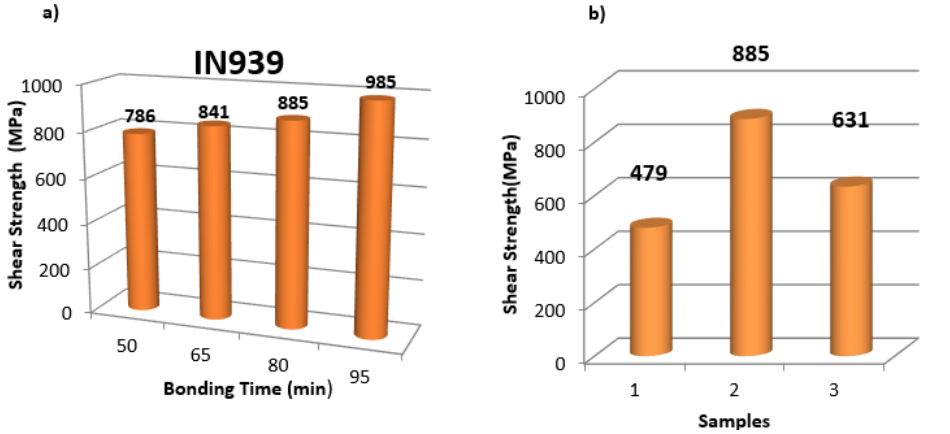

Figure 13. a) Shear strength for the similar IN939 TLP bonding using two step heating technique after heat treatment in different isothermal solidification time. b) Comparison of shear strength for similar joint IN939 (1) conventional TLP bonding at 80 min after heat treatment, (2) Two step TLP bonding at 80 min after heat treatment, (3) Two step TLP bonding at 80 min without heat treatment.

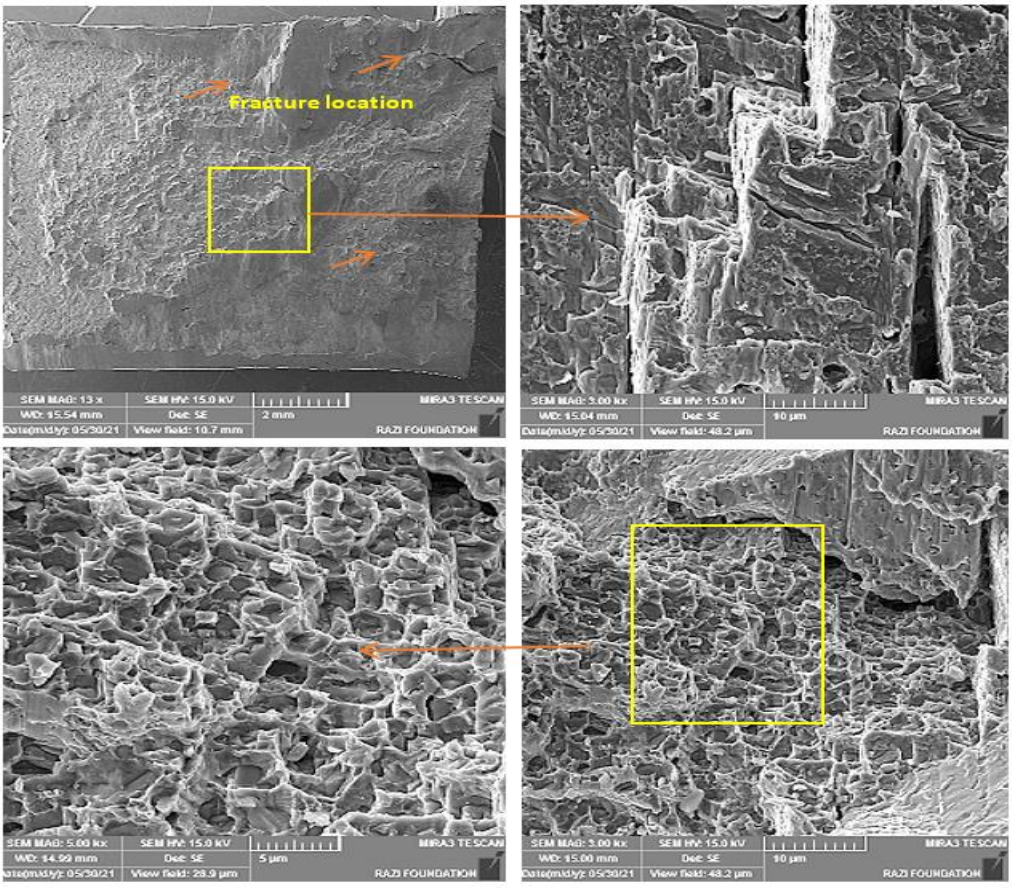

Figure 14. FE-SEM images for the fracture surface of shear test of the specimen D-80 without heat treatment

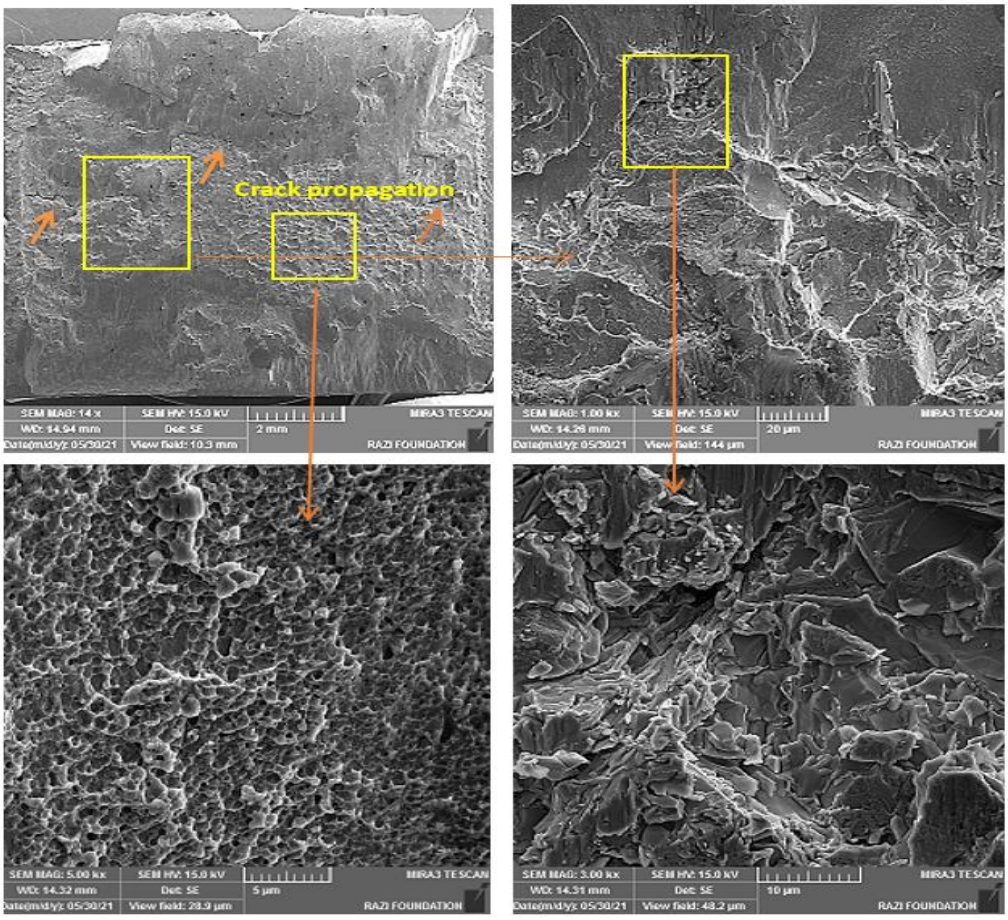

Figure 15. FE-SEM images for the fracture surface of shear test of the heat treated specimen D-80

4. CONCLUSIONS

From the results of two-step-heating technique and conventional TLP-bonding of IN939 superalloy in the present work, the following can be concluded:

1. By using two-step TLP bonding, the time needed to achieve isothermal solidification in TLP bonding was shortened.
2. If the athermal solidified zone (ASZ) is removed by prolonging the furnace's operation, the bond becomes ideal. The three main phases of eutectic products in ASZ are γ-solid solution, nickel and chromium-rich boride. Only the solid solution phase composed the isothermal solidification zone. Boride precipitates with needle and blocky shapes were found in the diffusion-affected zone.
3. The increased microhardness of the zones was related to hard, brittle boride precipitate particles in the DAZ and eutectic phases in the ASZ of all specimens. As bonding time increased, the microhardness of the isothermal solidified zone also increased. A post-bond heat treatment created a microstructure that was near the base metals and caused a homogenizing microstructure to develop across the joint.
4. The degree of formation of γ' on the bond line as opposed to the secondary phases in the polycrystalline substrate's diffusion zone had a larger effect on the shear strength of the bonds at room temperature. Fractography and bond shear tests both showed ductile shear failure at the bond line, which may have been caused by insufficient Gama-prime development within the joint, leaving a relatively soft bond line region. The second element that contributed to the development of brittle secondary fractures was the presence of second phases in the polycrystalline substrate's diffusion zone.

Data and code Availability

The datasets used and/or analyzed during the current study are available from the corresponding author (Ruaa Hatem Kadhim) on reasonable request.

Declaration

The authors declare that we have no known competing financial interests or personal relationships that could have appeared to influence the work reported in this paper.

Funding

The authors declare that no funds, grants, or other support were received during the preparation of this manuscript.

REFERENCES

[1] Kataria, R., Singh, R. P., Sharma, P., & Phanden, R. K. (2021). Welding of super alloys: a review. Materials Today: Proceedings, 38, 265-268.

[2] A. M. Jawarneh, F. M. AL-Oqla, A. Abu Jadoo, “Transient behavior of non-toxic natural and hybrid multi-layer desiccant composite materials for water extraction from atmospheric air”, Environmental Science and Pollution Research, Vol. 28, No. 33, 2021, pp.45609-45618.

[3] Fu, C., Chen, Y., Li, L., Antonov, S., & Feng, Q. (2020). Evaluation of service conditions of high pressure turbine blades made of DS Ni-base superalloy by artificial neural networks. Materials Today Communications, 22, 100838.

[4] BELKADDOUR, L., & BERRAHOU, M. (2022). Study of Repairing a Corroded Cryogenic Tank by Composite Wrap Subjected to Thermal and Mechanical Loadings. Jordan Journal of Mechanical and Industrial Engineering, 16(5).

[5] Shajari, Y., Razavi, S. H., Seyedraoufi, Z. S., & Samiee, M. (2021). The effect of time and temperature of solutionizing heat treatment on γ′ characterization in a Ni-base superalloy. Metallography, Microstructure, and Analysis, 10(4), 441-447.

[6] Al bkoor Alrawashdeh, K., Gharaibeh, N. S., Alshorman, A. A., & Okour, M. H. (2021). Magnus wind turbine effect vertical axis using rotating cylinder blades. Jordan Journal of Mechanical and Industrial Engineering, 15(2), 233-443.

[7] AL-Nafeay, R. H., AL-Roubaiy, A. O., & Omidvar, H. (2022). Finite Element Simulation of Thermal Residual Stress in TLP Bonding of Ni-base Superalloy.

[8] Sahoo, A., Tripathy, S., & Tripathy, D. K. (2022). Parametric Optimization of Pulse TIG Welding Process during Joining of Dissimilar Tensile Steels Used in Automotive Industries. Jordan Journal of Mechanical and Industrial Engineering, 16(5).

[9] Zhang, J. (2021). Design of Mechanical and Electrical Control System of Mixed Liquid Gas Pressure Energy Storage Based on Maximum Power Point Tracking. Jordan Journal of Mechanical and Industrial Engineering, 15(1).

[10] AL-Nafeay, R. H., AL-Roubaiy, A. O., & Omidvar, H. (2021, February). Overview of Joining and Repairing Techniques of Ni-Based Superalloy for Industrial Gas Turbine Applications. In IOP Conference Series: Materials Science and Engineering (Vol. 1094, No. 1, p. 012141). IOP Publishing.

[11] Duvall, D. S., Owczarski, W. A., & Paulonis, D. F. (1974), ―TLP bonding: a new method for joining heat resistant alloys‖, Weld. J.(NY), 53(4), 203-214.

[12] Soares, C. (2011), ―Gas turbines: a handbook of air, land and sea applications‖. Elsevier.

[13] Zhang, J. (2021). Design of Mechanical and Electrical Control System of Mixed Liquid Gas Pressure Energy Storage Based on Maximum Power Point Tracking. Jordan Journal of Mechanical and Industrial Engineering, 15(1).

[14] Sahraeian, R., Omidvar, H., Hadavi, S. M., Shakerin, S., & Maleki, V. (2018), ―An Investigation on High-Temperature Oxidation and Hot Corrosion Resistance Behavior of Coated TLP (Transient Liquid Phase)-Bonded IN738-LC‖. Transactions of the Indian Institute of Metals, 71(12), 2903-2918.

[15] Ismail, F. B., Al-Bazi, A., Al-Hadeethi, R. H., & Victor, M. (2021). A Machine Learning Approach for Fire-Fighting Detection in the Power Industry. Jordan Journal of Mechanical and Industrial Engineering, 15(5).

[16] MacDonald, W. D., & Eagar, T. W. (1992), ―Transient liquid phase bonding‖, Annual review of materials science, 22(1), 23-46.

[17] Shirzadi, A. A., & Wallach, E. R. (1997). Temperature gradient transient liquid phase diffusion bonding: a new method for joining advanced materials. Science and Technology of Welding and Joining, 2(3), 89-94.

[18] Wang, X., Li, X., & Yan, Q. (2007). A novel bonding process: Super-cooled transient liquid phase bonding. Acta Metallurgica Sinica(China), 43(10), 1096-1100.

[19] AMS 4777H: Nickel Alloy, Brazing Filler Metal, 82Ni-4.5Si-7.0Cr-3.1B-3.0Fe,1780 to 1830°F (971to 999°C) Solidus-Liquids Range, Aerospace Material Specification, SAE International, Warrendale, PA, 2010.

[20] M. J. Donachie (2002) "Superalloys: A technical guide, 2nd Edition," America (NY)., pp. 1–409.

[21] Shakerin, S., Omidvar, H., & Mirsalehi, S. E. (2016). "The effect of substrate's heat treatment on microstructural and mechanical evolution of transient liquid phase bonded IN-738 LC". Materials & Design, 89, 611-619.

[22] ASTM E384, Standard Test Method for Microindentation Hardness of Materials, ASTM International, 2009.

[23] Patricia B. Roy, Fiona M.O Connell (2013) Vickers Microindentation Hardness Testing of Brazed Joints in Aluminum, Loyola University Maryland, pp.1-20.

[24] Sadeghian, A., Arhami, F., & Mirsalehi, S. E. (2019). ―Phase formation during dissimilar transient liquid phase (TLP) bonding of IN939 to IN625 using a Ni-Cr-Fe-Si-B interlayer‖. Journal of Manufacturing Processes, 44, 72-80.

[25] Mousa, N. A., Alshadeedi, B. M., Attia, O. H., Mahmood, H. A., & Adam, N. M. (2022). Investigation of evaluated temperature oxidation for IN-738 LC superalloy turbine blade thermally coated by AL2O3 using slurry coating process. Eastern-European Journal of Enterprise Technologies, 3(12), 117.

[26] Arhami F, Mirsalehi SE, Sadeghian A, Johar MH.,(2019), The joint properties of a high chromium Ni-based superalloy made by diffusion brazing: microstructural evolution, corrosion resistance and mechanical behavior. J Manuf Process;37:203–11.

[27] Tokunaga, T., Nishio, K., Hasebe, M., 2001. Thermodynamic study of phase equilibria in the Ni-Si-B system. J. Phase Equilib. 22, 291–299.

[28] Hardwick, L., Rodgers, P., Pickering, E., & Goodall, R. (2021). Development of a novel Ni-based Multi-Principal Element Alloy filler metal, using an alternative melting point depressant. Metallurgical and Materials Transactions A, 52(6), 2534-2548.

[29] Al bkoor Alrawashdeh, K., Gharaibeh, N. S., Alshorman, A. A., & Okour, M. H. (2021). Magnus wind turbine effect vertical axis using rotating cylinder blades. Jordan Journal of Mechanical and Industrial Engineering, *15*(2), 233-443.

[30] Arhami F, Mirsalehi SE., (2019), The effect of heat treatment sequence on microstructure and mechanical properties of diffusion brazed IN-939 superalloy. J Mater Process Technol;266:351–62.

[31] Arhami, F., Mirsalehi, S. E., & Sadeghian, A. (2019). ―Effect of bonding time on microstructure and mechanical properties of diffusion brazed IN-939‖. Journal of Materials Processing Technology, 265, 219-229.

[32] Šulák, I., Babinský, T., Chlupová, A., Milovanović, A., & Náhlík, L. (2022). Effect of building direction and heat treatment on mechanical properties of Inconel 939 prepared by additive manufacturing. Journal of Mechanical Science and Technology, 1-6.

[33] Arhami, F., & Mirsalehi, S. E. (2018). Microstructural evolution and mechanical properties evaluation of IN-939 bonds made by isothermal solidification of a liquated Ni-Cr-B interlayer. Metallurgical and Materials Transactions A, 49(12), 6197-6214.

[34] Wang, X. G., X. G. Li, and C. G. Wang., (2012), "Transient liquid phase bonding of aluminium alloy using two-step heating process." Science and Technology of Welding and Joining 17.5: 414-418.

[35] Wang, X., Li, X., & Wang, C. (2013). ―Effect of two-step heating process on joint microstructure and properties during transient liquid phase bonding of dissimilar materials‖. Materials Science and Engineering: A, 560, 711-716.

[36] Wang, X. G., Li, X. G., & Yan, Q. (2007). Effect of two step heating process on joint microstructure and properties during transient liquid phase bonding. Science and Technology of Welding and Joining, 12(5), 455-459.

[37] A. A. Shirzadi and E. R. Wallach,(1999), ―Analytical modelling of transient liquid phase (TLP) diffusion bonding when a temperature gradient is imposed‖, Acta mater.47, 3551-3560.

[38] Wang, Xue Gang, and Xin Geng Li.,(2013), "Transient liquid phase bonding of T91 steel using two-step heating process." Advanced Materials Research. Vol. 712. Trans Tech Publications Ltd.

[39] Irawan, A. P., Fitriyana, D. F., Siregar, J. P., Cionita, T., Anggarina, P. T., Jaafar, J. B., ... & Manalu10, J. (2024). Influence of Post-Heat Treatment on the Characteristics of FeCrBMnSi Coating on Stainless Steel 304 Substrate Prepared by Twin Wire Arc Spray (TWAS) Method at Various Stand-off Distance. Jordan Journal of Mechanical and Industrial Engineering, 81(2).

[40] Adeyeri, M. K., Ayodeji, S. P., Outomilola, E. O., & Bako, J. O. (2020). Design of a Screw Conveyor for Transporting and Cooling Plantain Flour in a Process Plant. Jordan Journal of Mechanical and Industrial Engineering, 14(4).